UCLA
COMPUTATIONAL AND APPLIED MATHEMATICS

A Boundary Condition Capturing Method for Incompressible Flame Discontinuities

Duc Q. Nguyen
Ronald P. Fedkiw
Myungjoo Kang

June 2000

CAM Report 00-19

Department of Mathematics
University of California, Los Angeles
Los Angeles, CA. 90095-1555

http://www.math.ucla.edu/applied/cam/index.html

A Boundary Condition Capturing Method for Incompressible Flame Discontinuities

Duc Q. Nguyen *†
Ronald P. Fedkiw * ‡
Myungjoo Kang *†

June 15, 2000

Abstract

In this paper, we propose a new numerical method for treating two phase incompressible flow where one phase is being converted into the other, e.g. the vaporization of liquid water. We consider this numerical method in the context of treating discontinuously thin flame fronts for incompressible flow. This method was designed as an extension of the Ghost Fluid Method [4] and relies heavily on the boundary condition capturing technology developed in [13] for the variable coefficient Poisson equation and in [12] for multiphase incompressible flow. Our new numerical method admits a sharp interface representation similar to the method proposed in [9]. More importantly, the interface boundary conditions are handled in a simple and straightforward way making the code very robust, e.g. merging is trivial for our method. The method is presented in three spatial dimensions, with numerical examples in one, two and three spatial dimensions.

*Research supported in part by ONR N00014-97-1-0027

†Department of Mathematics, University of California Los Angeles, Los Angeles, California 90095

‡Computer Science Department, Stanford University, Stanford, California 94305

1 Introduction

Consider multiphase incompressible flow including the effects of viscosity, surface tension and gravity. Any numerical approach to this problem needs both a method for tracking (or capturing) the interface location as well as a method for enforcing the appropriate boundary conditions at the tracked interface. See [23], [1] and [19] (and [2]) for numerical methods that used front tracking, volume of fluid and level set methods, respectively, for tracking (or capturing) the location of the multiphase interface. All these methods use a δ-function formulation to enforce the appropriate boundary conditions at the multiphase interface. This δ-function formulation was originally proposed as part of the "immersed boundary" method for computing solutions to the incompressible Navier-Stokes equations in the presence of a submersed elastic interface, see [16] and [17]. The numerical methods in [23], [1], [19] and [2] all extend the δ-function formulation of [16] to treat multiphase incompressible flow.

One drawback of the δ-function formulation is that it smears out numerical quantities across the interface producing a continuous profile for the density, the viscosity and the pressure across the interface. This numerical smearing can be problematic, e.g. a continuous pressure profile does not adequately model surface tension forces and [23], [1], [19] and [2] need to add source terms to the right hand side of the momentum equations in order to numerically model these forces. An alternative strategy for enforcing the interface boundary conditions is based on the Ghost Fluid Method (GFM) of [4]. In [13], the authors extended the GFM to treat the variable coefficient Poisson equation in the presence of an immersed interface. In [12], the authors used the method from [13] to devise a numerical method for multiphase incompressible flow that allows for a nonsmeared numerical representation of the density, the viscosity and the pressure. Moreover, since surface tension was modeled directly with a jump in the pressure, the authors did not need to add source terms to the right hand side of the momentum equations as in [23], [1], [19] and [2].

For multiphase incompressible flow, the interface moves with local fluid velocity only and individual fluid particles do not cross the interface. In this paper, we consider interfaces where a reaction is taking place and the interface moves with the local unreacted fluid velocity plus a reaction term that accounts for the conversion of one fluid into the other. That is, we account for the movement of material across the interface. Consider for example an interface separating liquid and gas regions where the liquid is actively vaporizing into the gaseous state. See [11] for a front tracking approach to

this problem using a δ-function formulation to treat the interface boundary conditions. See [22] for a level set based, δ-function formulation of this same problem, and see [24] for a volume of fluid based approach. [11], [22] and [24] solve an equation for the temperature in order to determine the rate at which one material is converted into another. Another interesting example occurs in combustion. Assuming that the flame front is infinitely thin allows one to treat the flame front as a discontinuity separating two incompressible flows. The unreacted material undergoes reaction as it crosses the interface producing a lower density (higher volume) reacted material. See [20] for a front tracking approach to this problem using a δ-function formulation. The flame speeds in [20] were determined with the aid of the G-equation [14, 25], so an extra equation for the temperature was not needed.

In these problems, the density of the incompressible material tends to be different on different sides of the interface. Thus the material must instantaneously expand as it crosses the interface implying that the normal velocity is discontinuous across the interface as well, i.e. in addition to discontinuity of the density, the viscosity, and the pressure. The methods in [11], [22], [24] and [20] are all based on the $\delta-$function formulation and thus smear out this velocity jump. This can be quite problematic since this numerical smearing adds a compressible character to the flow field near the interface, i.e. the divergence free condition is not exactly satisfied in each separate subdomain. In addition, difficulties arise when trying to determine the interface velocity which depends in part on the local velocity of the unreacted material. Near the interface, the velocity of the unreacted material contains large $O(1)$ numerical errors where it has been nonphysically forced to be continuous with velocity of the reacted material. Partial solutions to these problems where proposed in [9] where the authors were able to remove the numerical smearing of the normal velocity obtaining a sharp interface profile. Unfortunately, the interface treatment in [9] was considerably intricate and the calculation had to be terminated if two flame fronts were significantly close to each other, i.e. this method cannot handle the simple merging of flame discontinuities. However, we note that this method was used to obtain rather impressive results in [10] for problems where the flames do not merge.

In this paper, we propose a new numerical method for treating two phase incompressible flow where one phase is being converted into the other. This method was designed as an extension of the Ghost Fluid Method [4] and relies heavily on the boundary condition capturing technology developed in [13] for the variable coefficient Poisson equation and in [12] for multiphase incompressible flow. Our new numerical method admits a sharp interface representation similar to the method proposed in [9]. More importantly, the

interface boundary conditions are handled in a simple and straightforward way making the code very robust, e.g. merging is trivial for our method. The method is outlined in three spatial dimensions, with numerical examples in one, two and three spatial dimensions.

2 Equations

2.1 Euler Equations

The basic equations for inviscid incompressible flow are,

$$\rho_t + \vec{V} \cdot \nabla \rho = 0 \tag{1}$$

$$u_t + \vec{V} \cdot \nabla u + \frac{p_x}{\rho} = 0 \tag{2}$$

$$v_t + \vec{V} \cdot \nabla v + \frac{p_y}{\rho} = 0 \tag{3}$$

$$w_t + \vec{V} \cdot \nabla w + \frac{p_z}{\rho} = 0 \tag{4}$$

where t is the time, (x, y, z) are the spatial coordinates, ρ is the density, $\vec{V} =< u, v, w >$ is the velocity field, p is the pressure and $\nabla = \left\langle \frac{\partial}{\partial x}, \frac{\partial}{\partial y}, \frac{\partial}{\partial z} \right\rangle$. In addition, the divergence free condition is $\nabla \cdot \vec{V} = 0$. The equations for the velocities can be written in condensed notation as a row vector

$$\vec{V} + \left(\vec{V} \cdot \nabla\right) \vec{V} + \frac{\nabla p}{\rho} = 0 \tag{5}$$

2.2 Interface Velocity

When treating multiphase incompressible flow, one needs an expression for the velocity, $\vec{W}$, of the multiphase interface. If the interface is a simple contact discontinuity, then the interface moves with the local fluid velocity only, i.e. $\vec{W} = \vec{V}$. Many numerical methods use only the normal velocity of the interface, i.e. $\vec{W} = D\vec{N}$ where D is the normal component of the interface velocity and $\vec{N} =< n_1, n_2, n_3 >$ is the local unit normal to the interface. In the case of a contact discontinuity, $D = V_N = \vec{V} \cdot \vec{N}$.

Throughout this text, *unreacted* and *reacted* incompressible flows are separated by an interface across which the unreacted material is converted to the reacted material, and "u" and "r" subscripts are used to refer to the unreacted and reacted materials, respectively. The normal component of the interface velocity is calculated by adding the unreacted local fluid velocity to the flame speed, S. That is, $D = (V_N)_u + S$ where $(V_N)_u$ is calculated using the velocity of the unreacted material only. This is important to note since V_N is discontinuous across the interface.

In the numerical examples, the flame speed is defined as $S = S_o + \sigma\kappa$ where S_o and σ are constants and κ is the local curvature of the interface.

2.3 Jump Conditions

Conservation of mass and momentum implies the standard Rankine-Hugoniot jump conditions across the interface

$$[\rho(V_N - D)] = 0 \tag{6}$$

$$\left[\rho(V_N - D)^2 + p\right] = 0 \tag{7}$$

where $[A] = A_r - A_u$ defines "$[\cdot]$" as the jump in a quantity across the interface. When $D \neq V_N$, the tangential velocities are continuous as well, i.e. $[V_{T_1}] = [V_{T_2}] = 0$ where T_1 and T_2 are the unit tangent vectors. This is true as long as $S \neq 0$, i.e. it is true as long as the front is not a contact discontinuity. Note that in the case of a contact discontinuity, i.e. $S = 0$, the tangential velocities are completely uncoupled across the interface and equations 6 and 7 reduce to $[V_N] = [p] = 0$. For more details, see [5].

Denoting the mass flux in the moving reference frame (speed D) by

$$M = \rho_r \left((V_N)_r - D\right) = \rho_u \left((V_N)_u - D\right) \tag{8}$$

allows equation 6 to be rewritten as $[M] = 0$. Furthermore,

$$M = -\rho_u S \tag{9}$$

follows from substituting $D = (V_N)_u + S$ into equation 8.

Starting with $[D] = 0$,

$$[V_N - (V_N - D)] = 0 \tag{10}$$

$$\left[\frac{\rho V_N - \rho(V_N - D)}{\rho}\right] = 0 \tag{11}$$

$$\left[\frac{\rho V_N - M}{\rho}\right] = 0 \tag{12}$$

and

$$[V_N] = M\left[\frac{1}{\rho}\right] \tag{13}$$

where the last equation follows since $[M] = 0$. It is more convenient to write

$$\left[\vec{V}\right] = M\left[\frac{1}{\rho}\right]\vec{N} \tag{14}$$

in place of equation 13 and $[V_{T_1}] = [V_{T_2}] = 0$. Taking the dot product of equation 14 and $\vec{N}$ results in equation 13, while taking the dot product of equation 14 and $\vec{T_1}$ or $\vec{T_2}$ results in $[V_{T_1}] = 0$ and $[V_{T_2}] = 0$ respectively.

Equation 7 can be rewritten as

$$\left[\frac{M^2}{\rho} + p\right] = 0 \tag{15}$$

or as

$$[p] = -M^2 \left[\frac{1}{\rho}\right] \tag{16}$$

again using $[M] = 0$.

2.4 Level Set Equation

The level set equation

$$\phi_t + \vec{W} \cdot \nabla\phi = 0 \tag{17}$$

is used to keep track of the interface location as the set of points where $\phi = 0$. The unreacted and reacted materials are then designated by the points where $\phi > 0$ and $\phi \leq 0$ respectively. Using $\phi \leq 0$ instead of $\phi = 0$ for the reacted points removes the measure zero ambiguity of points that happen to lie on the interface. In this sense, the numerical interface lies in between $\phi = 0$ and the positive values of ϕ and can be located numerically by finding the zero level of ϕ. To keep the values of ϕ close to those of a signed distance function, i.e. $|\nabla\phi| = 1$, the reinitialization equation

$$\phi_\tau + S(\phi_o)\left(|\nabla\phi| - 1\right) = 0 \tag{18}$$

is iterated for a few steps in ficticious time, τ. The level set function is used to compute the normal

$$\vec{N} = \frac{\nabla\phi}{|\nabla\phi|} \tag{19}$$

and the curvature

$$\kappa = -\nabla \cdot \vec{N} \tag{20}$$

in a standard fashion. For more details on the level set function see [4, 15, 19, 12].

3 Numerical Method

A standard MAC grid is used for discretization where $p_{i,j,k}$, $\rho_{i,j,k}$ and $\phi_{i,j,k}$ exist at the cell centers (grid points) and $u_{i\pm\frac{1}{2},j,k}$, $v_{i,j\pm\frac{1}{2},k}$, and $w_{i,j,k\pm\frac{1}{2}}$ exist at the appropriate cell walls. See [7] and [18] for more details.

3.1 Extending the Velocity Field

Since the normal velocity is discontinuous across the interface, one has to use caution when applying numerical discretizations near the interface. For example, when discretizing the unreacted fluid velocity near the interface, one should avoid using values of the reacted fluid velocity. Following the Ghost Fluid Methodology in [4], a band of ghost cells on the reacted side of the interface is populated with unreacted ghost velocities that can be used in the discretization of the unreacted fluid velocity. Similarly, reacted ghost velocities are defined on a band of ghost cells on the unreacted side of the interface and used in the discretization of the reacted fluid velocity.

ϕ is defined at the grid nodes, and its values on the offset MAC grid are computed with simple averaging, e.g. $\phi_{i+\frac{1}{2},j,k} = \frac{\phi_{i,j,k}+\phi_{i+1,j,k}}{2}$. The MAC grid values of ϕ can then be used to determine which values of the velocity field correspond to unreacted material and which correspond to reacted material. At each MAC grid location that corresponds to a reacted fluid velocity, the jump conditions in equation 14 are used to define a new unreacted ghost velocity according to

$$u_u^G = u_r - M\left(\frac{1}{\rho_r} - \frac{1}{\rho_u}\right) n_1 \tag{21}$$

$$v_u^G = v_r - M\left(\frac{1}{\rho_r} - \frac{1}{\rho_u}\right) n_2 \tag{22}$$

and

$$w_u^G = w_r - M\left(\frac{1}{\rho_r} - \frac{1}{\rho_u}\right) n_3 \tag{23}$$

where n_1, n_2 and n_3 are computed at the appropriate MAC grid locations using simple averaging, e.g. $(n_1)_{i+\frac{1}{2},j,k} = \frac{(n_1)_{i,j,k}+(n_1)_{i+1,j,k}}{2}$. Similarly, reacted ghost velocities are calculated at unreacted MAC grid locations using

$$u_r^G = u_u + M\left(\frac{1}{\rho_r} - \frac{1}{\rho_u}\right) n_1 \tag{24}$$

$$v_r^G = v_u + M\left(\frac{1}{\rho_r} - \frac{1}{\rho_u}\right) n_2 \tag{25}$$

and

$$w_r^G = w_u + M\left(\frac{1}{\rho_r} - \frac{1}{\rho_u}\right) n_3 \tag{26}$$

3.2 Level Set Equation

The level set function is evolved in time from ϕ^n to ϕ^{n+1} using nodal velocities, $\vec{W} = D\vec{N}$, where $\vec{N}$ is computed at each grid node using equation 19 as described in [12]. In general, $D = (V_N)_u + S$ where $(V_N)_u$ is the normal velocity of the unreacted material and $S = S_o + \sigma\kappa$ is the flame speed. If S depends on the local curvature of the front, i.e. $\sigma \neq 0$, then $\vec{W}$ is split into a purely convective component $\vec{W}_c = ((V_N)_u + S_o)\,\vec{N}$ and a curvature component $\sigma\kappa\vec{N}$ allowing equation 17 to be rewritten as

$$\phi_t + \vec{W}_c \cdot \nabla\phi = -\sigma\kappa|\nabla\phi| \tag{27}$$

where the curvature term is isolated on the right hand side. Then κ is discretized according to equation 20 as discussed in [12], and $|\nabla\phi|$ is discretized with standard central differencing.

The normal velocity of the unreacted material, $(V_N)_u$, is needed in a band about the front so that equation 27 can be solved locally to update the interface location. The nodal values of the unreacted velocity, $\vec{V}_u$, are determined using simple averaging of the MAC grid values making use of the appropriate ghost values (defined above) where needed, i.e. $u_{i,j,k} = \frac{u_{i-\frac{1}{2},j,k}+u_{i+\frac{1}{2},j,k}}{2}$, $v_{i,j,k} = \frac{v_{i,j-\frac{1}{2},k}+v_{i,j+\frac{1}{2},k}}{2}$, and $w_{i,j,k} = \frac{w_{i,j,k-\frac{1}{2}}+w_{i,j,k+\frac{1}{2}}}{2}$ are used to calculate the nodal values of the unreacted velocity. Then $(V_N)_u = \vec{V}_u \cdot \vec{N}$ is used to define the unreacted normal velocity at each grid node.

Detailed discretizations for convective part of equation 27, i.e. $\vec{W}_c \cdot \nabla\phi$, and for equation 18 are given in [4]. Note that the 5th order WENO discretization from [4] is used to discretize the convective part of equation 27 and the spatial terms in equation 18 for the numerical examples in this paper.

3.3 Projection Method

First, $\vec{V}^\star = \langle u^\star, v^\star, w^\star \rangle$ is defined by

$$\frac{\vec{V}^\star - \vec{V}^n}{\triangle t} + \left(\vec{V} \cdot \nabla\right)\vec{V} = 0 \tag{28}$$

and then the velocity field at the new time step, $\vec{V}^{n+1} = \langle u^{n+1}, v^{n+1}, w^{n+1} \rangle$, is defined by

$$\frac{\vec{V}^{n+1} - \vec{V}^{\star}}{\triangle t} + \frac{\nabla p}{\rho} = 0 \tag{29}$$

so that combining equations 28 and 29 to eliminate $\vec{V}^{\star}$ results in equation 5. Taking the divergence of equation 29 results in

$$\nabla \cdot \left(\frac{\nabla p}{\rho} \right) = \frac{\nabla \cdot \vec{V}^{\star}}{\triangle t} \tag{30}$$

after setting $\nabla \cdot \vec{V}^{n+1}$ to zero. Equations 29 and 30 can be rewritten as

$$\vec{V}^{n+1} - \vec{V}^{\star} + \frac{\nabla p^{\star}}{\rho} = 0 \tag{31}$$

and

$$\nabla \cdot \left(\frac{\nabla p^{\star}}{\rho} \right) = \nabla \cdot \vec{V}^{\star} \tag{32}$$

eliminating their dependence on $\triangle t$ by using a scaled pressure, $p^{\star} = p \triangle t$. See [3], [7] and [18] for more details.

3.4 Convection Terms

The MAC grid stores u values at $\vec{x}_{i\pm\frac{1}{2},j,k}$. Updating $u^{\star}_{i\pm\frac{1}{2},j,k}$ in equation 28 requires the discretization of $\vec{V} \cdot \nabla u$ at $\vec{x}_{i\pm\frac{1}{2},j,k}$. First, simple averaging can be used to define $\vec{V}$ at $\vec{x}_{i\pm\frac{1}{2},j,k}$. For example

$$v_{i+\frac{1}{2},j,k} = \frac{v_{i,j-\frac{1}{2},k} + v_{i,j+\frac{1}{2},k} + v_{i+1,j-\frac{1}{2},k} + v_{i+1,j+\frac{1}{2},k}}{4} \tag{33}$$

and

$$w_{i+\frac{1}{2},j,k} = \frac{w_{i,j,k-\frac{1}{2}} + w_{i,j,k+\frac{1}{2}} + w_{i+1,j,k-\frac{1}{2}} + w_{i+1,j,k+\frac{1}{2}}}{4} \tag{34}$$

define v and w at $\vec{x}_{i+\frac{1}{2},j,k}$ while u is already defined there. Then the $\vec{V} \cdot \nabla u$ term on the offset $\vec{x}_{i\pm\frac{1}{2},j,k}$ grid can be discretized in the same fashion as the $\vec{V} \cdot \nabla \phi$ term on the regular $\vec{x}_{i,j,k}$ grid using the method outlined in [4]

for equation 17. $v^{\star}_{i,j\pm\frac{1}{2},k}$ and $w^{\star}_{i,j,k\pm\frac{1}{2}}$ are updated in a similar manner. For more details see [12]. Note that the 3rd order ENO discretization from [4] is used in the examples section.

It is important to note that the ghost values of the extended velocity field are used in this discretization of $\vec{V}^{\star}$. That is, unreacted fluid velocities are discretized with the aid of the unreacted ghost velocities avoiding the use of any reacted velocities that would pollute the solution. Similarly the reacted fluid velocities are are discretized using their ghost values avoiding the unreacted fluid velocities in the discretization.

Once again using the GFM philosophy [4], values for $\vec{V}^{\star}_u$ and $\vec{V}^{\star}_r$ are determined on the appropriate side of the interface *and* on a band including the interface. For example, $\vec{V}^{\star}_u$ is computed on both the unreacted side of the interface and on a band of ghost cells on the reacted side of the interface. This is done to alleviate problems that occur when the interface moves through the grid changing the character of the solution from unreacted to reacted or vice versa. As the interface moves, as dictated by the evolution of ϕ^n to ϕ^{n+1}, one always has appropriate values for $\vec{V}^{\star}_u$ and $\vec{V}^{\star}_r$ where needed.

3.5 Poisson Equation

Once $\vec{V}^{\star}$ has been updated with equation 28, the right hand side of equation 32 is discretized using standard central differencing, e.g.

$$(u^{\star}_x)_{i,j,k} = \frac{u^{\star}_{i+\frac{1}{2},j,k} - u^{\star}_{i-\frac{1}{2},j,k}}{\triangle x} \tag{35}$$

is used to compute $u^{\star}_x$. Once again, note that the ghost values of the extended velocity fields are used to compute these derivatives so that unreacted and reacted velocities are not mixed. Then the techniques presented in [13] for the variable coefficient Poisson equation are used to solve equation 32 for the pressure at the grid nodes. The resulting pressure is used to find $\vec{V}^{n+1}$ in equation 31 taking care to compute the derivatives of the pressure in *exactly* the same way as they were computed in equation 32 using the techniques in [13].

The techniques in [13] require a level set function to describe the interface location. We use ϕ^{n+1} as opposed to ϕ^n, since we wish to find the pressure that will make $\vec{V}^{n+1}$ divergence free in equation 31. This implies that both equation 31 and equation 32 should use $\rho^{n+1} = \rho(\phi^{n+1})$ in order to determine when to use ρ_u or ρ_r.

Note that one can set $\left[\frac{p_x}{\rho}\right] = \left[\frac{p_y}{\rho}\right] = \left[\frac{p_z}{\rho}\right] = 0$ when solving the Poisson equation using the method in [13]. Since the full equations 2, 3 and 4 are

continuous across the interface, one can take the divergence of the full equations without considering jump conditions. On the other hand, the jump in pressure defined in equation 16 needs to be accounted for when solving the Poisson equation with the method in [13]. Equation 16 is rewritten as

$$[p^\star] = -\triangle t M^2 \left(\frac{1}{\rho_r} - \frac{1}{\rho_u} \right) \tag{36}$$

for use equation 32. The $[p^\star]$ is computed at each grid node.

After discretizing the Poisson equation for the pressure, the resulting system of linear equations is solved with a preconditioned conjugate gradient (PCG) method using an Incomplete Choleski preconditioner [6]. The PCG algorithm is applied once for every Euler time step, or a total of three times for a third order Runge Kutta cycle.

3.6 Runge Kutta

Since both second and third order TVD Runge Kutta schemes [21] can be written as a convex combination of simple Euler steps, see [21, 12], it is straightforward to generalize the first order time discretization discussed so far to third order TVD Runge Kutta. One difficulty in implementing Runge Kutta methods in problems with interfaces arises when nodal values change character as the interface moves (e.g. one may inadvertently average unreacted and reacted velocity values). However, the use of the Ghost Fluid Method circumvents this difficulty.

While the values of the level set can be averaged directly, one has to be careful when averaging the velocity field in order to ensure that unreacted and reacted velocities are not accidently averaged together. Initially, $\vec{V}_u$ is defined on one side of the interface and $\vec{V}_r$ is defined on the other. Each of these velocity fields can be extended to a band about the interface using the appropriate jump conditions as outlined above. It is straightforward to use equation 28 to obtain $\vec{V}_u^\star$ and $\vec{V}_r^\star$ in the appropriate locations including a band about the interface. However, solving equation 29 for $\vec{V}_u^{n+1}$ and $\vec{V}_r^{n+1}$ only gives updated velocity values on the appropriate side of the interface and does not give valid values for $\vec{V}_u^{n+1}$ and $\vec{V}_r^{n+1}$ on a band including the interface. If the time n values and time $n+1$ values represent different Runge Kutta stages, they cannot be averaged unless the time $n+1$ values are extended to include a band about the interface. Luckily, we can easily extend these values to a band about the interface using our standard velocity extension procedure outlined above. The point is, that one should apply

Runge Kutta averaging to the extended velocity fields in order to avoid unwanted errors due to mixing the unreacted and reacted velocity fields.

3.7 Adaptive Time Stepping

Adaptive time stepping is used where the overall time step is chosen as the minimum of the incompressible time step and the level set time step, i.e.

$$\triangle t = .5 \min(\triangle t^I, \triangle t^L) \tag{37}$$

where we have chosen a CFL restriction of .5. For incompressible flow, the convective time step restriction

$$\triangle t^I \left(\frac{|u|}{\triangle x} + \frac{|v|}{\triangle y} + \frac{|w|}{\triangle z} \right) \leq 1 \tag{38}$$

needs to be satisfied at every grid point. For the level set equation, i.e. equation 27, the convective time step restriction

$$\triangle t^L \left(C_{cfl} + K_{cfl} \right) \leq 1 \tag{39}$$

needs to be satisfied at every grid point where

$$C_{cfl} = \frac{|w_1|}{\triangle x} + \frac{|w_2|}{\triangle y} + \frac{|w_3|}{\triangle z} \tag{40}$$

with $\vec{W}_c =< w_1, w_2, w_3 >$ is for the convection terms and

$$K_{cfl} = \sigma \left(\frac{2}{(\triangle x)^2} + \frac{2}{(\triangle y)^2} + \frac{2}{(\triangle z)^2} \right) \tag{41}$$

is for the curvature terms.

4 Examples

Note that in the one dimensional examples, the Conjugate Gradient method is used without the Incomplete Choleski preconditioner, since the Incomplete Choleski factorization does not work in the one dimensional case. All of the two dimensional examples utilize the PCG method with the Incomplete Choleski preconditioner. Unless otherwise specified, the unreacted and reacted densities are $\rho_u = 1$ and $\rho_r = .2$, respectively.

4.1 One Spatial Dimension

All of the one dimensional examples are computed with 100 grid points on a $[-1, 1]$ domain. Exact solutions are shown as solid lines in the figures.

4.1.1 Example 1

Consider a flame with speed $S = 1$ initially located at $x = 0$. The unreacted gas flows in from the right with a velocity of $u = -1$. A Dirichlet, $p = 0$, boundary condition is specified on the left hand side of the domain, and a Neumann pressure boundary condition is used on the right hand side of the domain to keep the inflow velocity fixed. Figure 1 shows the computed solution for this stationary flame. The calculation for figure 1 may seem rather trivial, since the initial data is already the exact solution. In figure 2, the same calculation is carried out starting with erroneous initial data. Even with this poor initial guess, the correct solution is obtained. Note that the inflow velocity was still $u = -1$.

4.1.2 Example 2

Consider two flames both with speed $S = 1$ initially located at $x = -.5$ and $x = .5$. The unreacted material is at rest in the center of the domain. Dirichlet, $p = 0$, boundary conditions are specified at both ends of the the domain. Initially, the reacted velocities on the left and right hand sides of the domain were specified as $u = -4$ and $u = 4$ respectively. Figure 3 shows the computed velocity, and illustrates the ability of our algorithm to treat merging in one dimension. After merging, the domain contains a single phase incompressible fluid which must have a constant velocity. In the case of compressible flow, a finite speed of propagation rarefaction wave would lower the velocity to the average of the two reacted velocities (zero in this case). For incompressible flow, the "rarefaction" wave moves at infinite

speed and the velocity drops to zero in one time step as shown in the figure 3.

4.1.3 Example 3

Consider two flames both with speed $S = 1$ initially located at $x = -.5$ and $x = .5$. The reacted material is at rest in the center of the domain and the unreacted material is flowing in with speed $|u| = 4$ from both boundaries. Dirichlet, $p = 0$, boundary conditions are specified at both ends of the domain. Figure 4 shows the computed solution.

4.2 Two Spatial Dimensions

4.2.1 Example 4

Consider two planar flames both with speed $S = 1$ initially located at $x = .25$ and $x = .75$ in a $[0,1] \times [0,1]$ domain with the unreacted material at rest in the center of the domain. Dirichlet, $p = 0$, boundary conditions were used on the right and left hand sides of the domain, i.e. in the x-direction, and periodic boundary conditions were used in the y-direction. Initially, the reacted velocities on the left and right hand sides of the domain were specified as $\vec{V} =< -4, 0 >$ and $\vec{V} =< 4, 0 >$ respectively. This example is the two dimensional equivalent of example 2 above and illustrates the merging of two planar flames in two spatial dimensions. Results for the x component of the velocity field are shown in figures 5 using a computational mesh with 50 grid cells in each direction.

4.2.2 Example 5

In this example we consider the Darrieus-Landau instability with $S = 1$ in a $[0, \frac{2\pi}{5}] \times [0, \frac{2\pi}{5}]$ domain with 60 grid cells in each direction. The initial flame profile is a small amplitude cosine wave defined by $y = .005\cos(5x) + \frac{\pi}{5}$. The unreacted material is flowing in from the bottom of the domain with an initial velocity of $\vec{V} =< 0, 1 >$ and the reacted material flowing out of the top of the domain with an initial velocity of $\vec{V} =< 0, 5 >$. Dirichlet, $p = 0$, boundary conditions were used in the y-direction, and periodic boundary conditions were used in the x-direction. The initial values of $|\phi|$ were determined by placing $10,000$ equally (x-direction) spaced points on the flame front and computing the minimum distance from this set of points to each Cartesian grid location where the values of the level set are stored.

The sign of ϕ was calculated by comparing each Cartesian grid location to $y = .005\cos(5x) + \frac{\pi}{5}$.

The Darrieus-Landau instability results in exponential growth of the amplitude of the flame, $A(t) = A_o exp(\omega t)$, where

$$\omega = \frac{k|M|}{\rho_u + \rho_r}\left(\sqrt{1 + \frac{\rho_u}{\rho_r} - \frac{\rho_r}{\rho_u}} - 1\right) \tag{42}$$

is the rate of exponential growth, e.g. see [9]. Figure 6 shows a plot of amplitude versus time (labeled $q = 5$ where $q = \frac{\rho_u}{\rho_b}$) as compared to the exact solution. Initially there is some disagreement, since we did not start out with the exact Darrieus-Landau velocity field, but instead used a piecewise constant approximation based on a planar flame profile as outlined above. Others have noticed this same initial transient when using a planar approximation for the initial velocity field [8]. Figure 6 shows the results with $\rho_r = \frac{1}{4}$ (labeled $q = 4$) and $\rho_r = \frac{1}{3}$ (labeled $q = 3$) respectively. Note that the initial outflow velocity was changed to $\vec{V} =< 0, 4 >$ for the $q = 4$ case and to $\vec{V} =< 0, 3 >$ for the $q = 3$ case.

Figure 7 shows the time evolution of the flame front for a large amplitude perturbation defined by $y = .2\cos(5x) + \frac{\pi}{5}$ for the $q = 5$ case. The velocity field at the final time of $t = .2$ seconds is shown in figure 8. The gas flow converges toward the cusp and diverges away from the cusp, and the normal component of the velocity field is appropriately discontinuous. Note that the completely continuous velocity field shown in figure 6 of [20] damps out the severity of the converging to diverging nature of the velocity field as it crosses the interface near the cusp.

4.2.3 Example 6

Consider a planar flame located at $y = 7$ in a $[0, 5] \times [0, 10]$ domain. The unreacted material is below $y = 7$ and is initially at rest while the reacted material is flowing out of the top of the domain with an initial velocity of $\vec{V} =< 0, 4 >$. Dirichlet, $p = 0$, boundary conditions were used on the top of the domain and fixed velocity Neumann boundary conditions were used on the bottom of the domain. Periodic boundary conditions were used in the x-direction. To suppress the hydrodynamic instability development at short wavelengths, a curvature term was added to the flame speed to obtain $S = 1 + .1\kappa$.

In order to simulate flame vortex interaction, an infinite array of Oseen vortices were added to the unreacted material centered at spatial locations of $(x, y) = (2.5 + 5k, 5.5)$ where k is an integer. This adds only one vortex

to the computational domain at $(x, y) = (2.5, 5.5)$, and accounts for the periodicity of the domain in the x-direction. Vortices very far away have little effect on the computational domain so our initial data only accounts for the velocity prescribed by the vortices with $-500 \leq k \leq 500$. Each vortex is best expressed in polar coordinates with zero velocity in the radial direction and

$$V_\theta = \frac{1.5}{2\pi r}\left(1 - exp(-\frac{r^2}{.5^2})\right) \tag{43}$$

in the counterclockwise angular direction where r is the distance from the vortex core. The initial velocity of the unreacted material is determined by summing the contribution from each of the 1001 vortices considered. See [20] for more details.

Figure 9 shows the time evolution of the flame front for a 140 by 280 grid cell computation illustrating how the counterclockwise vortices distort the flame front. In figure 10 we show the results compared to those obtained after one level and two levels of grid coarsening. Note the first order accurate convergence for the flame location.

4.2.4 Example 7

Consider two circular flames centered at $(x, y) = (.6, .5)$ and $(x, y) = (.9, .5)$ both with radius $r = .1$ in a $[0, 1.5] \times [0, 1]$ domain with the reacted material inside the circles and the unreacted material outside the circles. The flame speed is given by $S = 1 + .01\kappa$, and Dirichlet, $p = 0$, boundary conditions were used on all sides of the domain. Figure 11 shows the time evolution of the flame front for a 60 by 40 grid cell computation. Figures 12, 13 and 14 show the velocity fields at different points in time. Note that the topological change (merging) requires no special treatment. Figure 15 shows the computation results for the 60 by 40 grid cell computation along with those obtained after one level and two levels of grid refinement. Note the first order accurate convergence for the flame location.

4.3 Three Spatial Dimensions

4.3.1 Example 8

Consider two spherical flames centered at $(x, y, z) = (.6, .5, .5)$ and $(x, y, z) = (.9, .5, .5)$ both with radius $r = .1$ in a $[0, 1.5] \times [0, 1] \times [0, 1]$ domain with the reacted material inside the spheres and the unreacted material outside

the spheres. The flame speed is given by $S = 1 + .01\kappa$, and Dirichlet, $p = 0$, boundary conditions were used on all sides of the domain. This is the three dimensional equivalent of example 7. Figures 16, 17 and 18 show the flame front at three different points in time for a 90 by 60 by 60 grid cell calculation illustrating the ease of merging in three spatial dimensions.

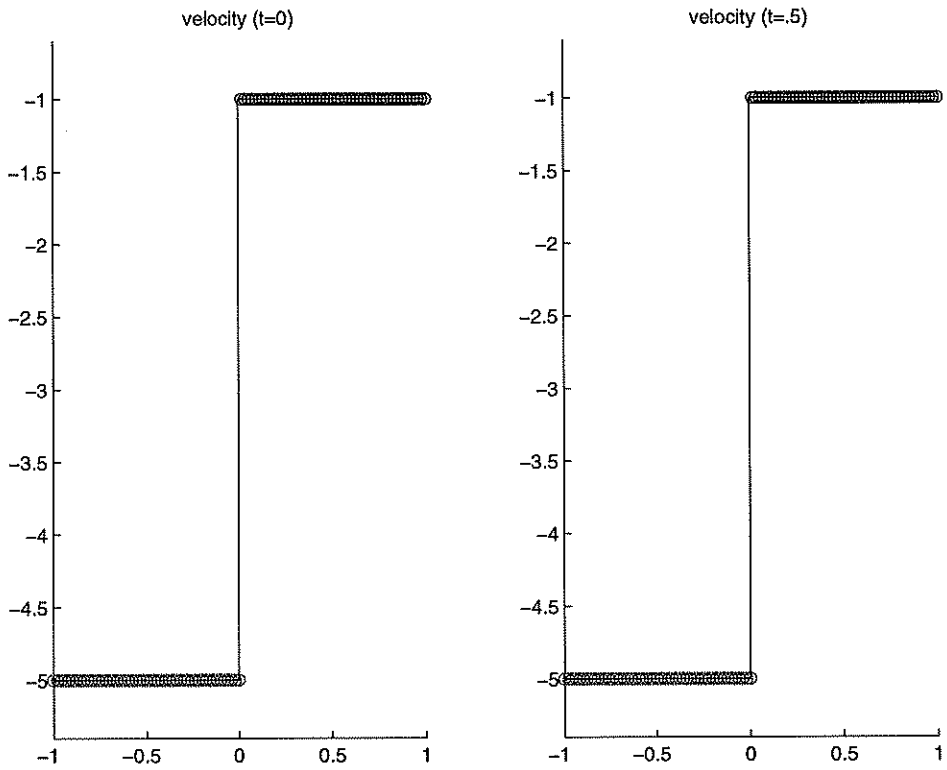

Figure 1: Stationary flame.

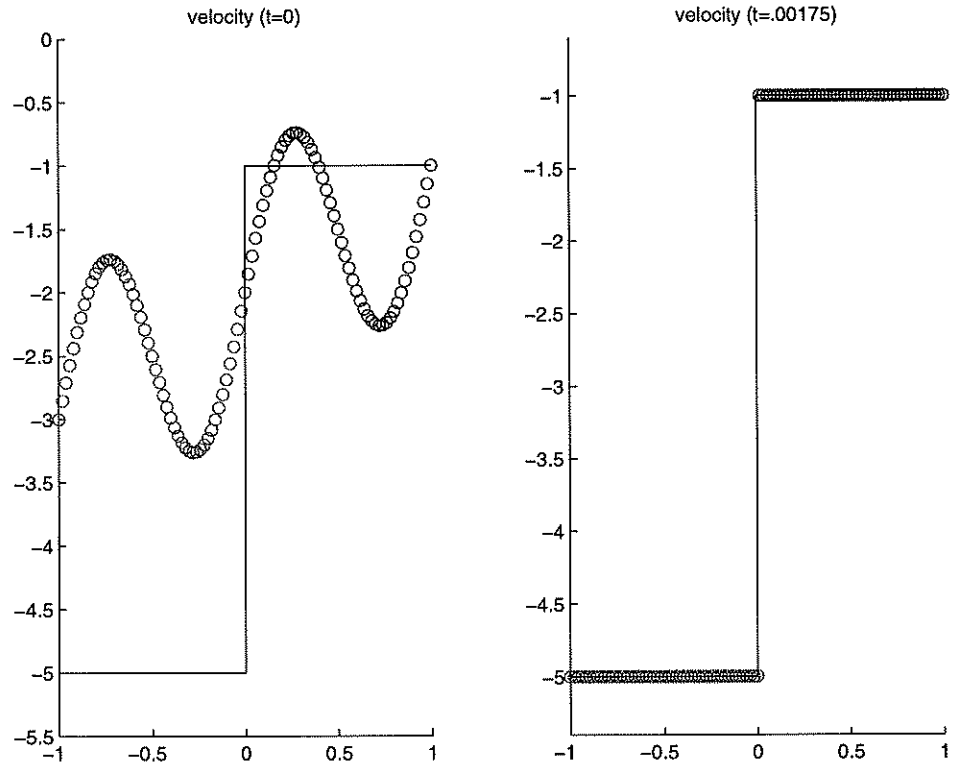

Figure 2: Stationary flame with a poor choice of initial data.

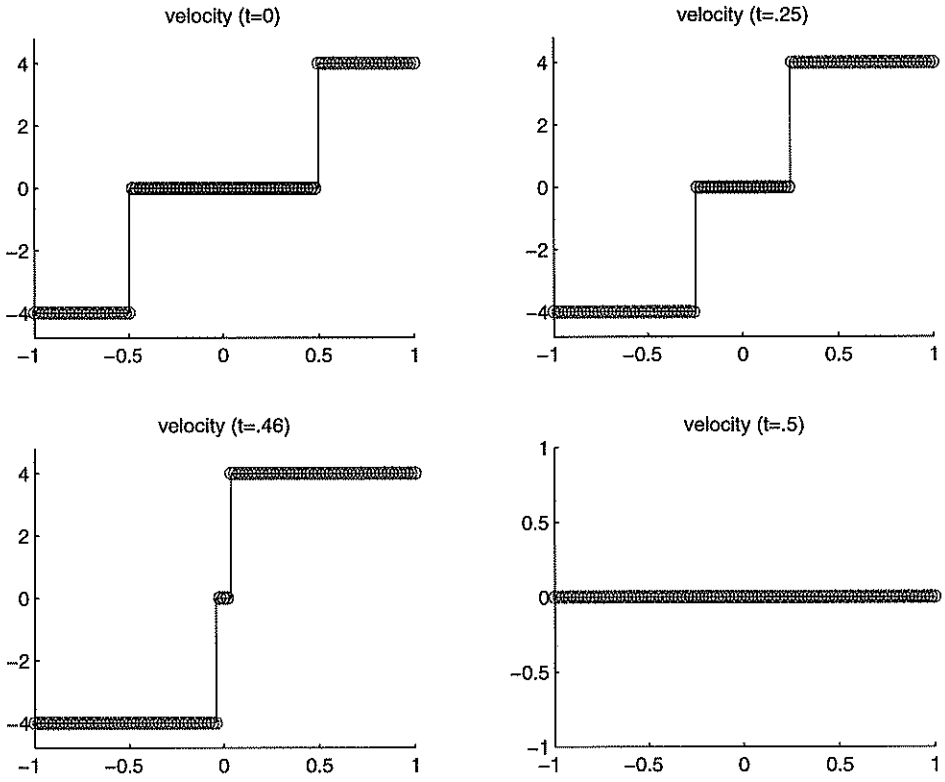

Figure 3: Merging flames.

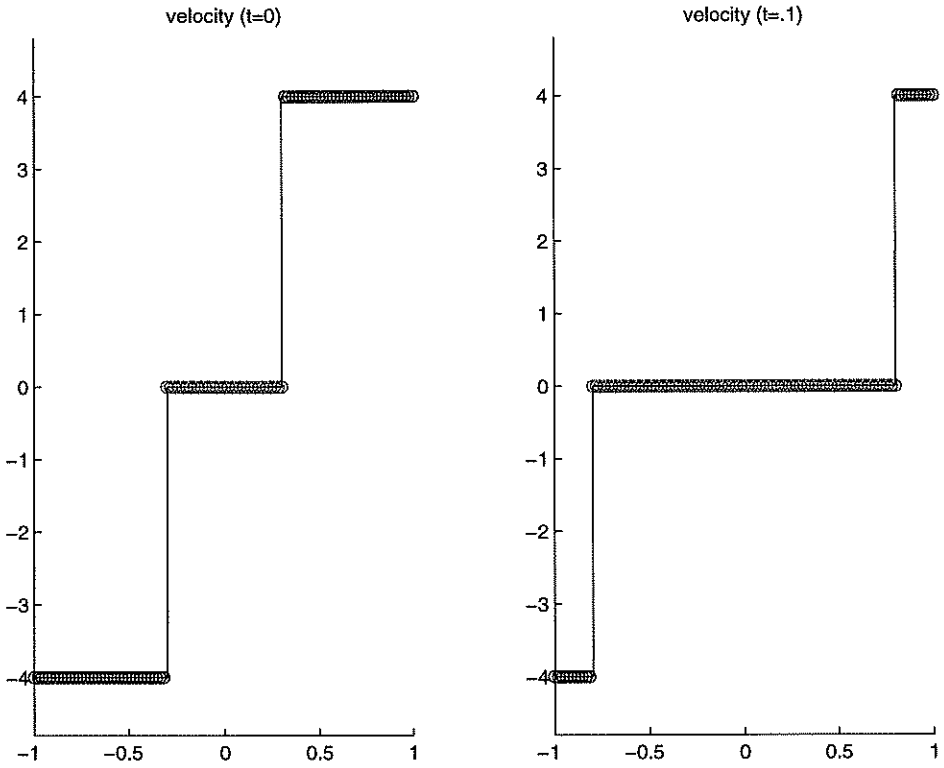

Figure 4: Separating flames.

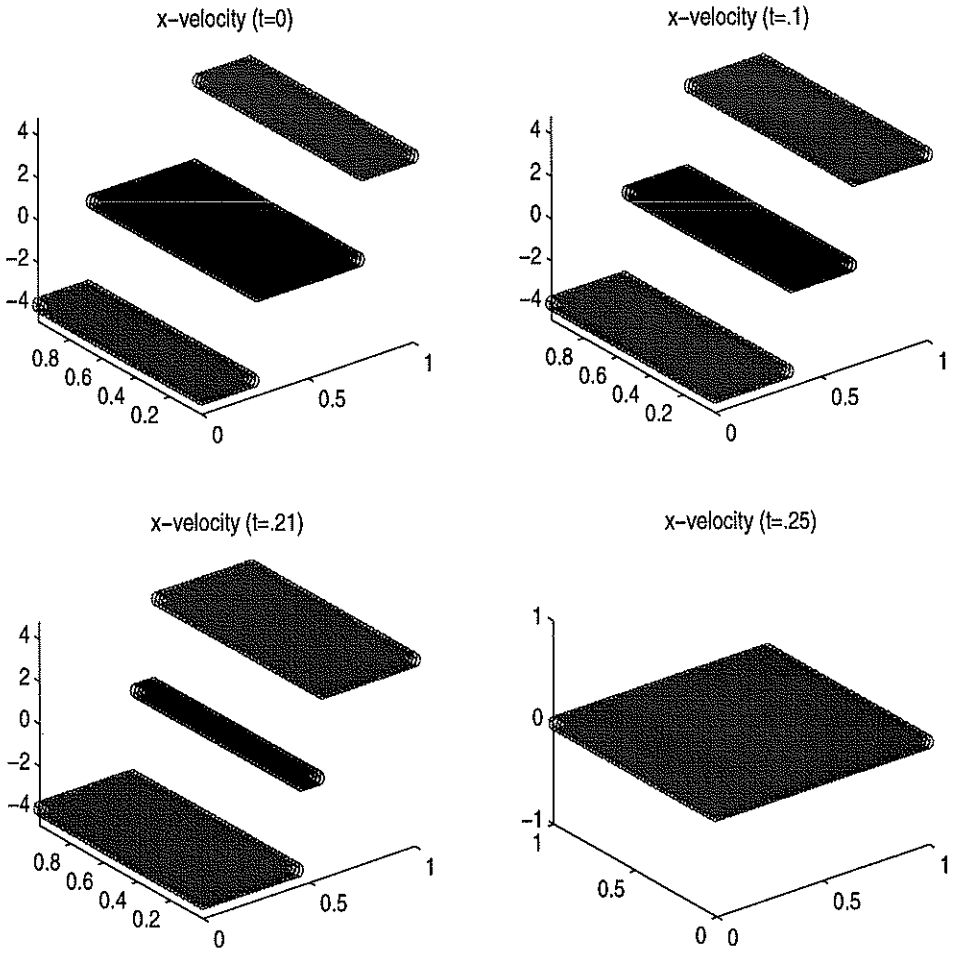

Figure 5: Merging planar flames in two spatial dimensions.

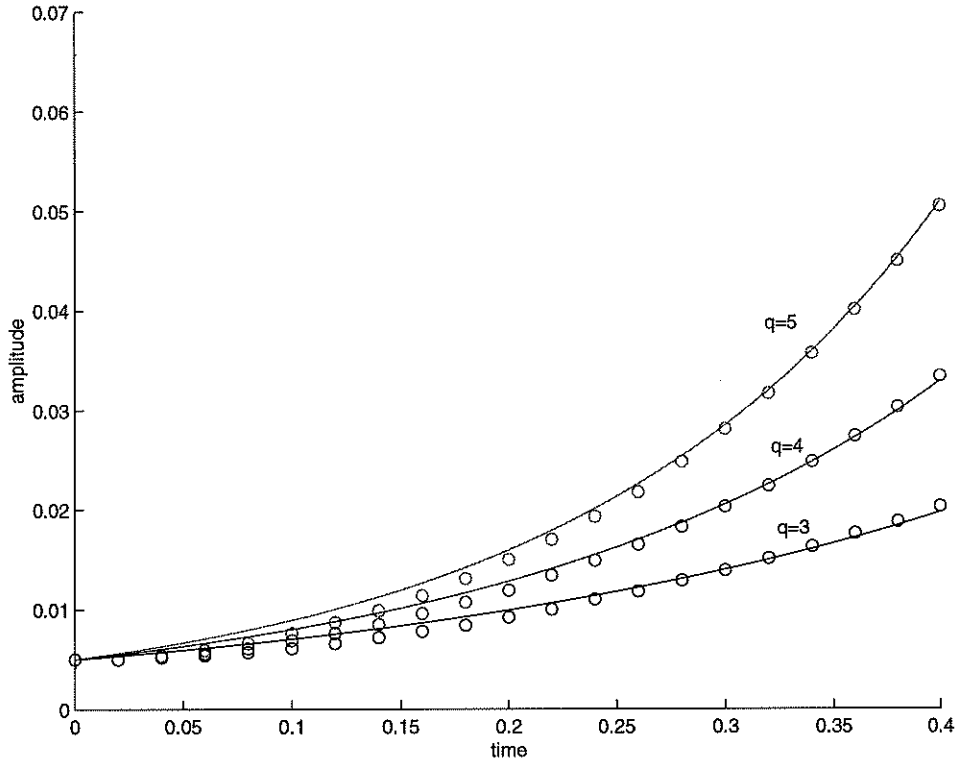

Figure 6: Darrieus-Landau instability - exponential growth of the amplitude.

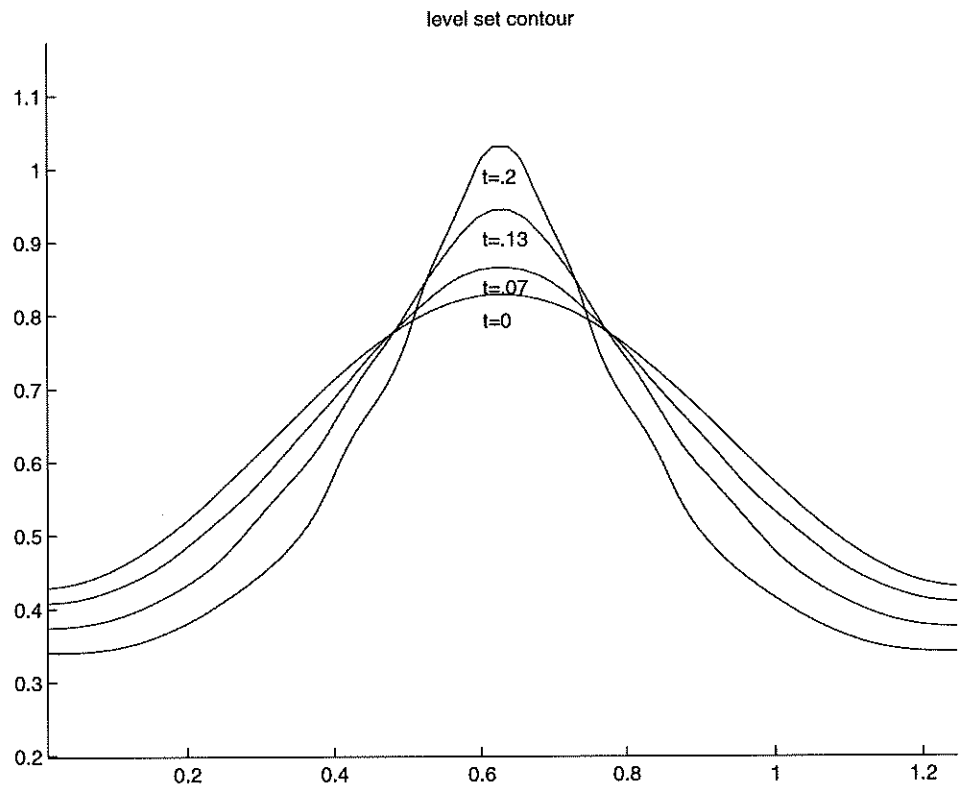

Figure 7: Large amplitude perturbation - time evolution.

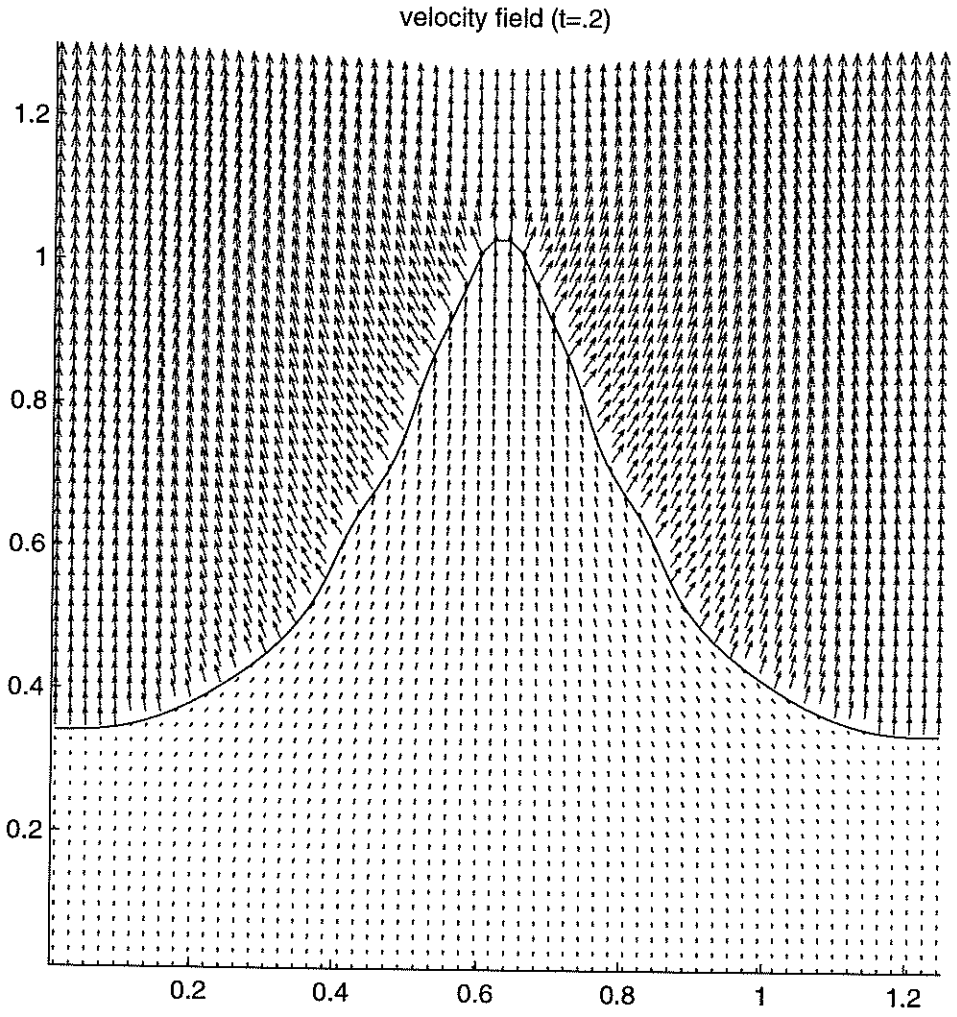

Figure 8: Large amplitude perturbation - converging to diverging velocity field with a discontinuous normal velocity across the interface.

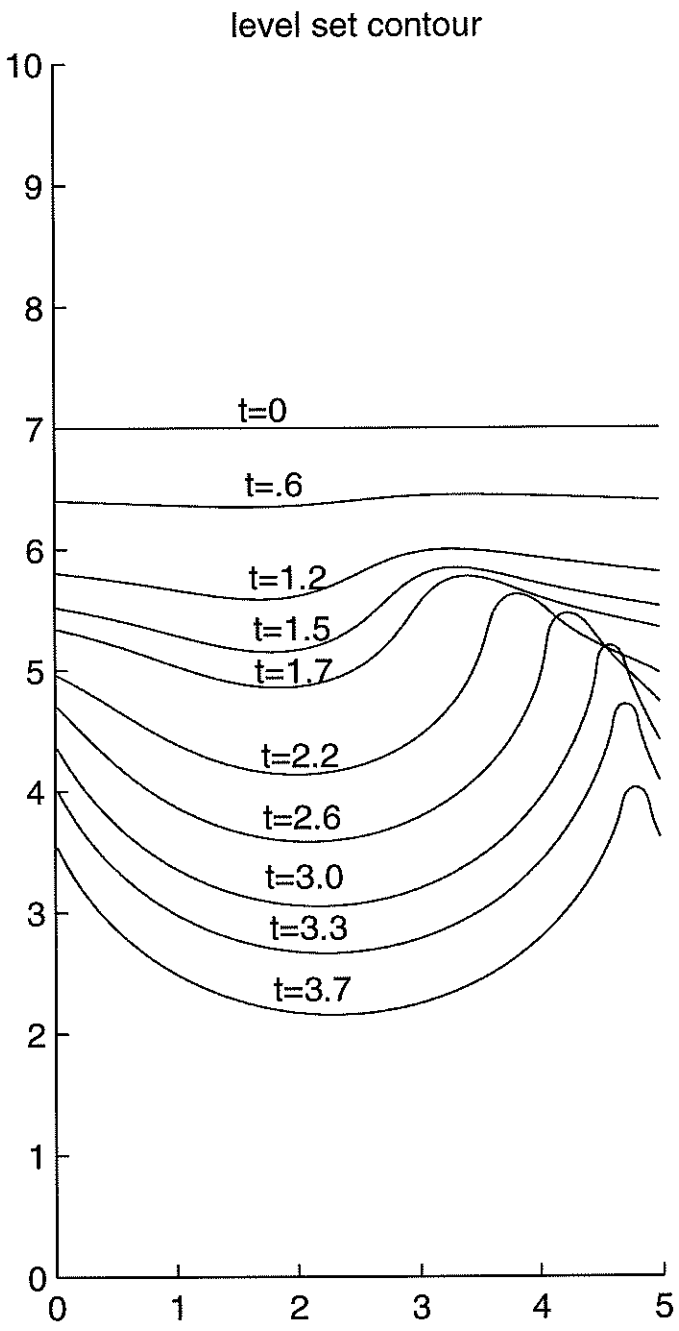

Figure 9: Flame vortex interaction - time evolution.

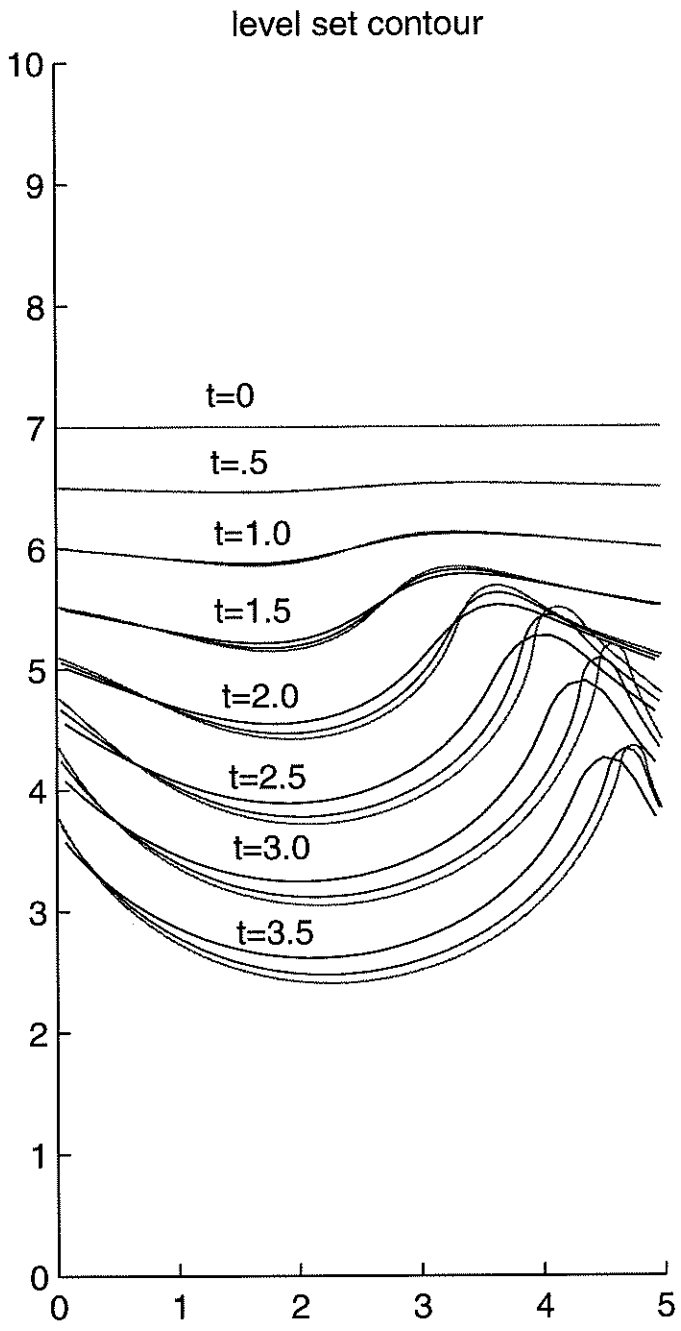

Figure 10: Flame vortex interaction - grid refinement.

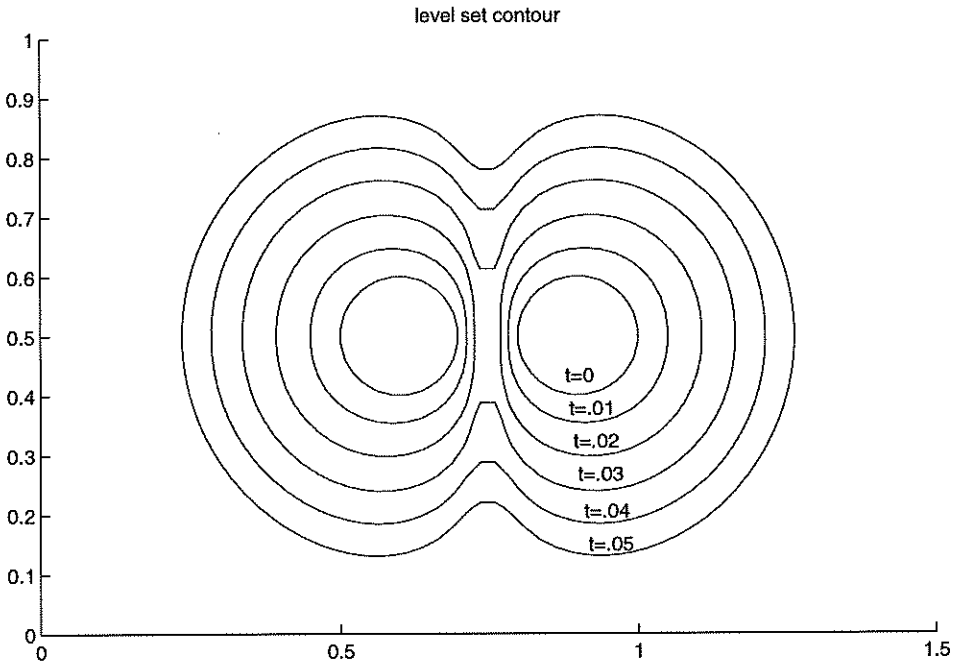

Figure 11: Merging circular flames - time evolution of the flame location.

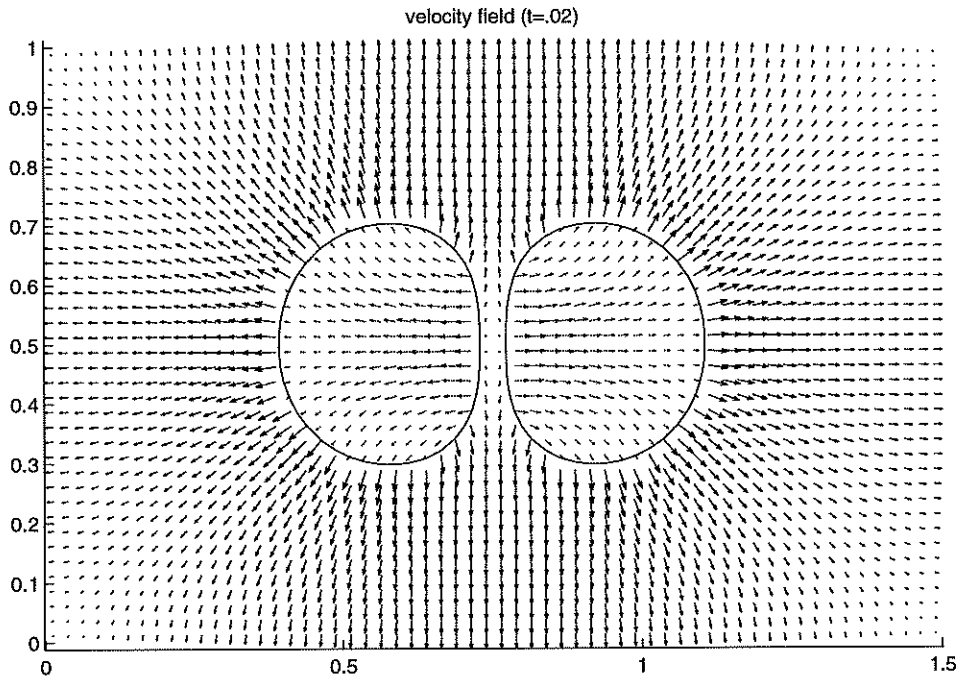

Figure 12: Merging circular flames - velocity field before merging.

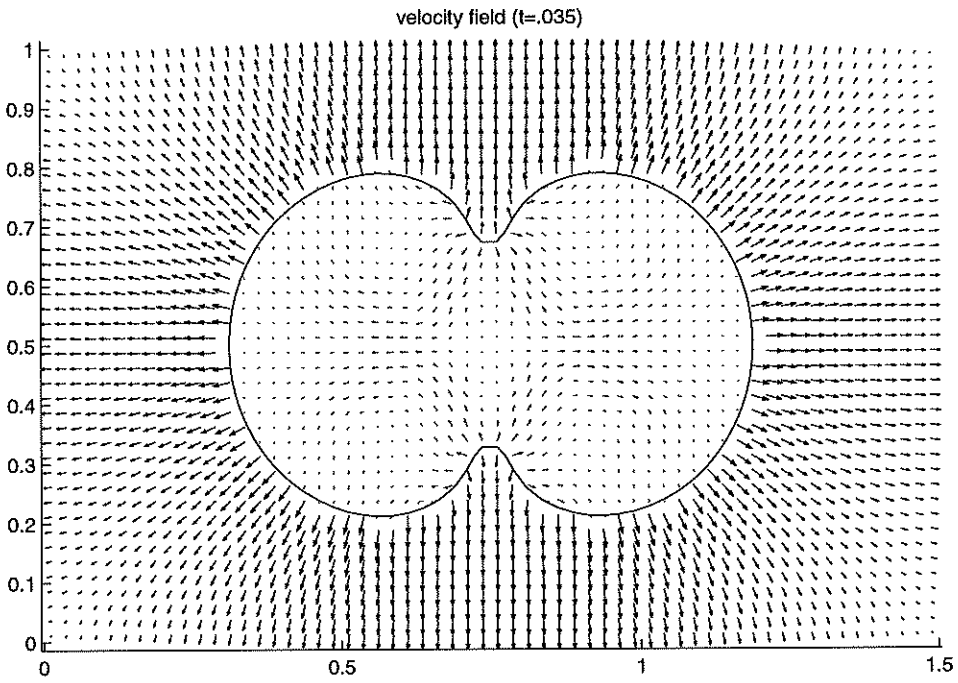

Figure 13: Merging circular flames - velocity field after merging.

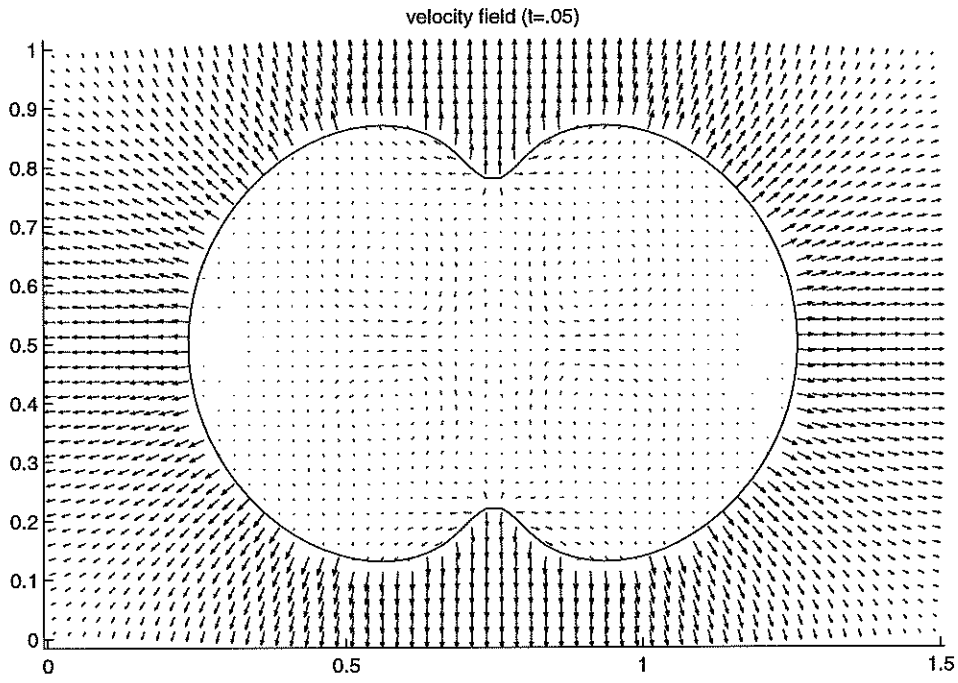

Figure 14: Merging circular flames - velocity field later in time.

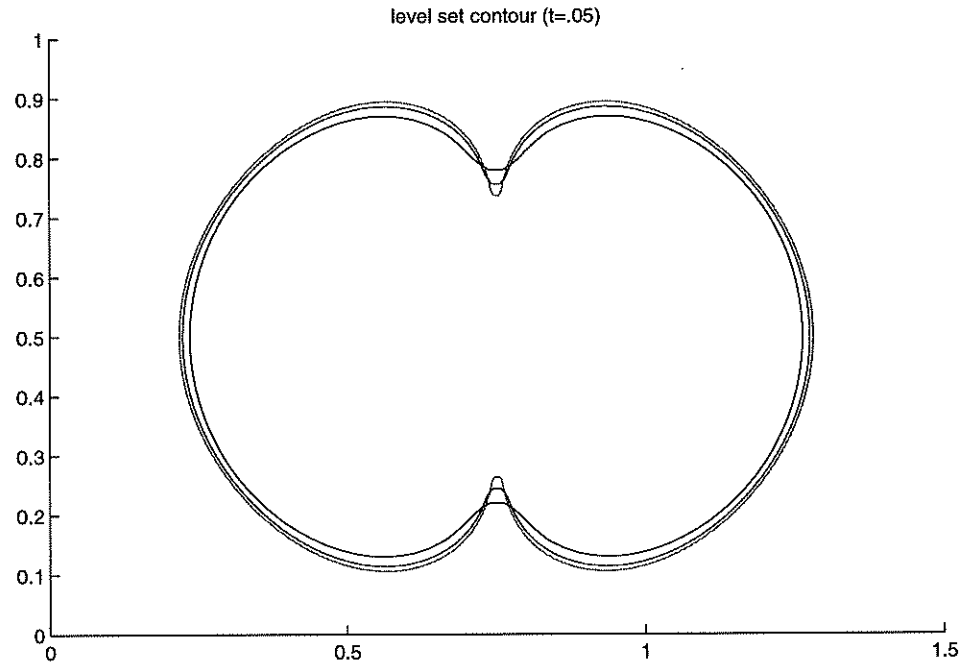

Figure 15: Merging circular flames - grid refinement demonstrating first order accuracy in the flame location.

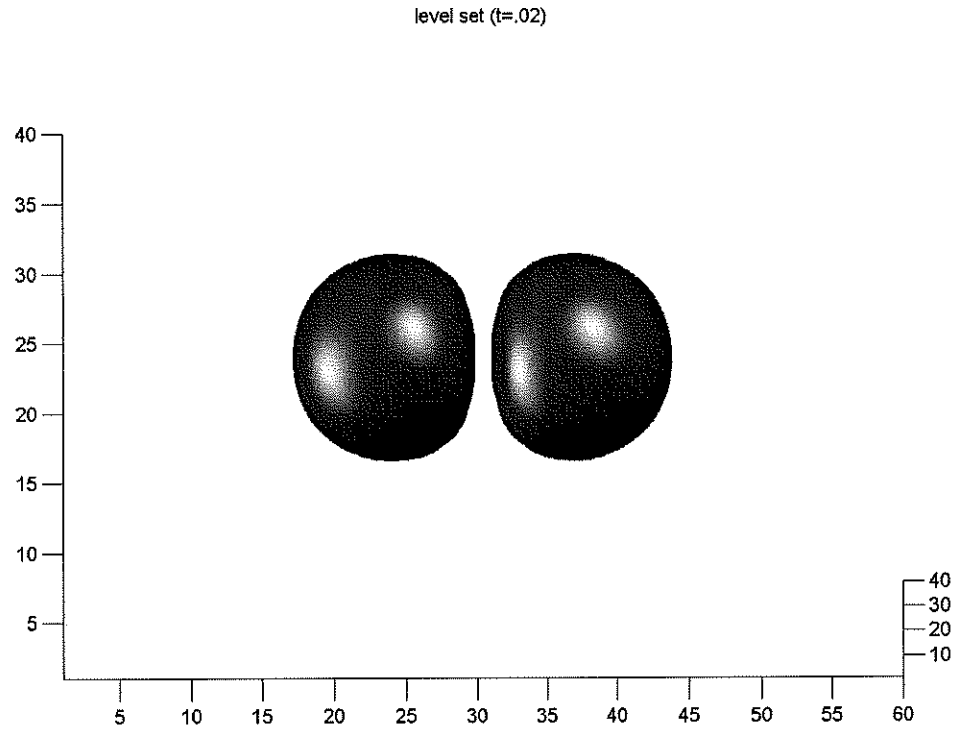

Figure 16: Merging spherical flames - flame location before merging.

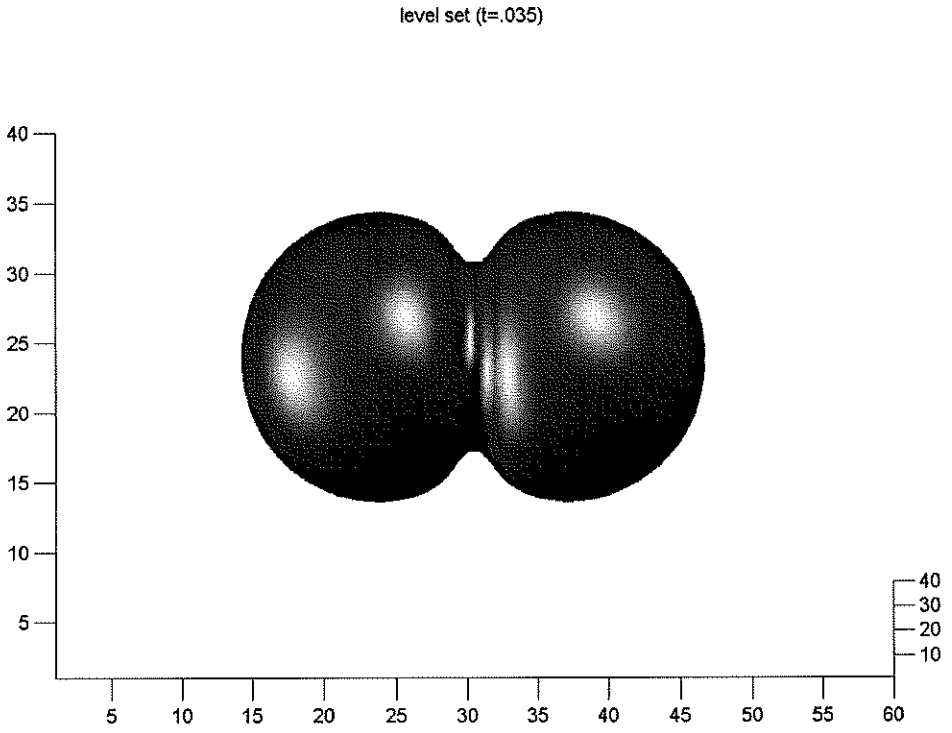

Figure 17: Merging spherical flames - flame location after merging.

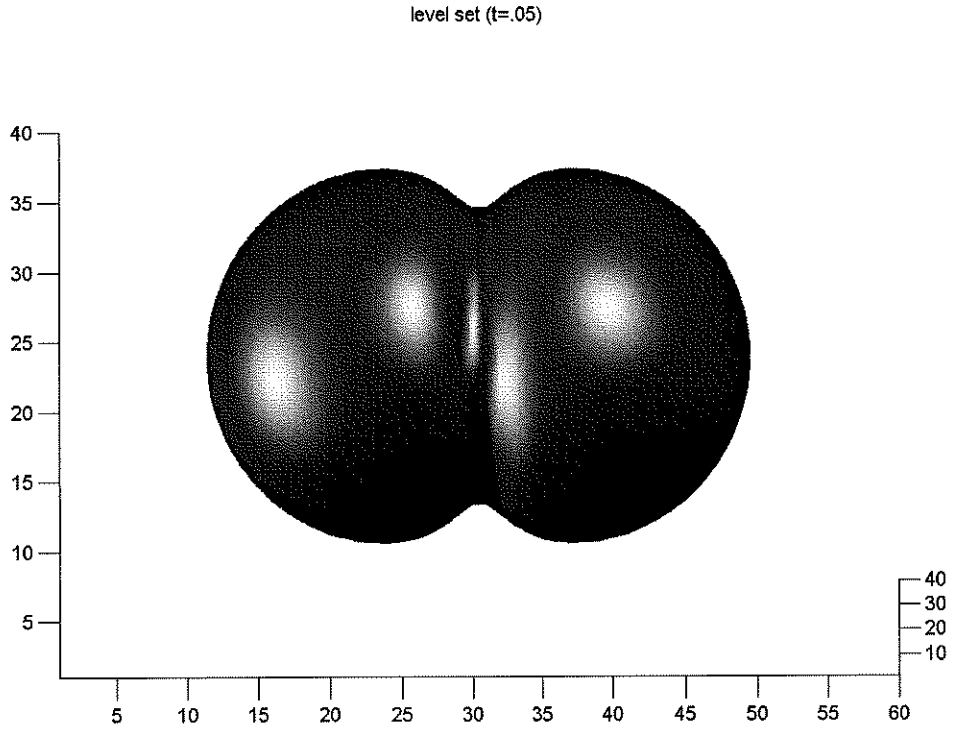

Figure 18: Merging spherical flames - flame location later in time.

References

[1] Brackbill, J.U., Kothe, D.B. and Zemach, C., *A Continuum Method for Modeling Surface Tension*, J. Comput. Phys. 100, 335-354 (1992).

[2] Chang, Y.C., Hou, T.Y., Merriman, B. and Osher, S., *A Level Set Formulation of Eulerian Interface Capturing Methods for Incompressible Fluid Flows*, J. Comput. Phys. 124, 449-464 (1996).

[3] Chorin, A.J. *Numerical Solution of the Navier-Stokes Equations*, Math. Comp. 22, 745-762 (1968).

[4] Fedkiw, R., Aslam, T., Merriman, B., and Osher, S., *A Non-Oscillatory Eulerian Approach to Interfaces in Multimaterial Flows (The Ghost Fluid Method)*, J. Comput. Phys. 152 (2), 457-492 (1999).

[5] Fedkiw, R., Aslam, T., and Xu, S., *The Ghost Fluid Method for Deflagration and Detonation Discontinuities*, J. Comput. Phys. 154, 393-427 (1999).

[6] Golub, G. and Van Loan, C., *Matrix Computations*, The Johns Hopkins University Press, Baltimore, 1989.

[7] Harlow, F.H. and Welch, J.E. *Numerical Calculation of Time-Dependent Viscous Incompressible Flow of Fluid with a Free Surface*, The Physics of Fluids 8, 2182-2189 (1965).

[8] Helenbrook, B.T., personal communication.

[9] Helenbrook, B.T., Martinelli, L. and Law, C.K. *A Numerical Method for Solving Incompressible Flow Problems with a Surface of Discontinuity*, J. Comput. Phys. 148, 366-396 (1999).

[10] Helenbrook, B.T and Law, C.K. *The Role of Landau-Darrieus Instabilty in Large Scale Flows*, Combustion and Flame 117, 155-169 (1999).

[11] Juric, D. and Tryggvason, G., *Computations of Boiling Flows*, Int. J. Multiphase Flow 24 (3), 387-410 (1998).

[12] Kang, M., Fedkiw, R., and Liu, X.-D., *A Boundary Condition Capturing Method for Multiphase Incompressible Flow*, J. Comput. Phys. (in review).

[13] Liu, X.-D., Fedkiw, R.P and Kang, M., *A Boundary Condition Capturing Method for Poisson's Equation on Irregular Domains*, J. Comput. Phys. 154, 151-178 (2000).

[14] Markstein, G.H., *Nonsteady Flame Propagation*, Pergamon Press, Oxford (1964).

[15] Osher, S. and Sethian, J.A., *Fronts Propagating with Curvature Dependent Speed: Algorithms Based on Hamilton-Jacobi Formulations*, J. Comput. Phys. 79, 12-49 (1988).

[16] Peskin, C., *Numerical Analysis of Blood Flow in the Heart*, J. Comput. Phys. 25, 220-252 (1977).

[17] Peskin, C. and Printz, B., *Improved Volume Conservation in the Computation of Flows with Immersed Elastic Boundaries*, J. Comput. Phys. 105, 33-46 (1993).

[18] Peyret, R. and Taylor, T.D., *Computational Methods for Fluid Flow*, Springer-Verlag, NY, 1983.

[19] Sussman, M., Smereka, P. and Osher, S., *A level set approach for computing solutions to incompressible two-phase flow*, J. Comput. Phys. 114, 146-154 (1994).

[20] Qian, J., Tryggvason, G. and Law, C.K. *A Front Method for the Motion of Premixed Flames*, J. Comput. Phys. 144, 52-69 (1998).

[21] Shu, C.W. and Osher, S., *Efficient Implementation of Essentially Non-Oscillatory Shock Capturing Schemes*, J. Comput. Phys. 77, 439-471 (1988).

[22] Son, G. and Dir, V.K. *Numerical Simulation of Film Boiling near Critical Pressures with a Level Set Method*, J. Heat Transfer 1221, 623-631 (1999).

[23] Unverdi, S.O. and Tryggvason, G., *A Front-Tracking Method for Viscous, Incompressible, Multi-Fluid Flows*, J. Comput. Phys. 100, 25-37 (1992).

[24] Welch, S. and Wilson, J., *A Volume of Fluid Based Method for Fluid Flows with Phase Change*, J. Comput. Phys. 160, 662-682 (2000).

[25] Williams, F.A., *The Mathematics of Combustion*, (J.D. Buckmaster, ed.), SIAM, Philadelphia, PA, pp. 97-131 (1985).